

Study on Silicon-Based Conformal Microstrip Angular Log-Periodic Meander Line Traveling Wave Tube

Tenglong He, Zhanliang Wang, Xinyi Li, Hexin Wang, Wei Shao, Hanwen Tian,
Lingna Yue, Huarong Gong, Zhaoyun Duan, Yanyu Wei, and Yubin Gong*

Abstract—Angular log-periodic meander line (ALPML) traveling wave tube (TWT) is one kind of low voltage miniature TWT. In order to decrease high frequency loss, avoid charge accumulation and enhance coupling impedance, the conformal microstrip ALPML TWT based on silicon substrate is proposed in this paper, which means that the projections of silicon supporting structure and metallic microstrip meander line are same in the top view. The microfabrication technology DRIE can be used to fabricate this structure. Compared with the conventional microstrip ALPML TWT, the coupling impedance of conformal microstrip ALPML TWT increases 50%. The particle-in-cell (PIC) simulation results reveal that the output power of conformal microstrip ALPML TWT can reach 220 W at 35 GHz, while the efficiency is 20%. The 3-dB bandwidth reaches 14 GHz in the frequency range between 28 GHz and 41 GHz when the operating voltage and radial sheet beam current are 3600 V and 0.3 A, respectively.

1. INTRODUCTION

With the explosion of mobile devices and wireless communication services, spectrum crisis is looming [1], which occurs in low frequency spectrum of the last generation communication technology. The new generation communication technology selects the underutilized millimeter wave frequency spectrum to be the next communication band [2]. With the technology development of new generation communication, there would be an urgent demand for the power devices at millimeter wave band. In earlier generation wireless communication technologies, the first choice of power source is solid state devices which have the advantages of compact dimensions and are easy to integrate [3]. However, the new communication technology puts forward new requirements for power source, which should be replaceable, has small size, broad bandwidth and high output power [4]. For vacuum electron devices, TWT is an important kind for wireless communication system at millimeter wave band due to high power, broad bandwidth and long lifespan. Compared with solid state devices, the main disadvantages of TWT are large dimensions and high operation voltage. Therefore, the miniaturization of TWT and voltage decreasing become a research hot spot and attract the industry interest.

Microstrip slow wave structure (SWS) is an optional type of SWS in miniature TWT, such as U-shaped and V-shaped microstrip meander line SWS [5]. Although the dimensions of microstrip SWS are smaller than that of the helix and coupled cavity SWS [6, 7], the voltage of microstrip SWS is still relatively high. To further reduce the operation voltage, the microstrip logarithmic spiral SWS is proposed in [8]. The logarithmic spiral SWS ($r = ae^{b\varphi}$) has low voltage as 40 V and a wide bandwidth. It cannot reach a large output power and high efficiency; meanwhile, the electronic optical system for focusing the radial sheet beam is difficult to design. Once raising the logarithmic parameter b for increasing the operation voltage, the dimension of structure will also increase, and the operation

Received 7 September 2018, Accepted 13 October 2018, Scheduled 24 October 2018

* Corresponding author: Yu-Bin Gong (ybgong@uestc.edu.cn).

The authors are with the National Key Laboratory of Science and Technology on Vacuum Electronics, School of Electronic Science and Engineering, University of Electronic Science and Technology of China, Chengdu 610054, China.

frequency will decrease. Therefore, this microstrip logarithmical spiral SWS is not applicable to high frequency wave band. In order to increase the operating frequency, the microstrip ALPML SWS was proposed in [9]. At Ka-band, it retains the advantages of small dimensions and relatively low operation voltage.

The proposed microstrip ALPML mentioned in [9, 10] consists of a winding metal strip on the top of a planar dielectric substrate. The planar dielectric substrate not covered by the microstrip meander lines would influence the interaction between the electromagnetic wave and electron beam. When electromagnetic wave propagates in conventional microstrip ALPML SWS, the electric field is concentrated on the planar dielectric substrate and its surface. Thus, conventional microstrip ALPML SWS has low coupling impedance. Furthermore, on account of planar structure and the accuracy of fabrication and assembling of the radial electron optical system [11], the deformed electron beam would unavoidably hit the exposed dielectric substrate under the practical situation, causing the charge accumulation, which would induce the electric discharge phenomena and make the SWS unstable.

One method for eliminating charge accumulation impact is reported in [12]. A dielectric-embedded microstrip meander-line (MML) SWS was proposed. The dielectric rod partly embedded in the metal replaces the dielectric substrate as upholder for meander-line. 3-D printing method was used to fabricate this kind of structure. However, this kind of structure still faced the fabricating difficulty. The material density and fastness of component cannot be ensured using laser sinter technology, and the fabricating accuracy is hard to reach the demand of vacuum electron devices. So, the method mentioned in [12] cannot guarantee the structure stability in vacuum environment.

In this paper, a conformal microstrip angular log-periodic meander line SWS is proposed. As shown in Fig. 1, the dielectric substrate where the microstrip meander lines do not cover will be removed, and the remaining dielectric substrate has the same shape as the metallization layer. Then, the loss of dielectric substrate will be decreased and electric flux density above metal layer increased [13]. In reality, the conformal microstrip ALPML SWS based on the silicon can be fabricated by means of the deep reaction ion etching method (DRIE). DRIE as a microfabrication technology has higher fabricating accuracy and parallel fabrication capacity of multiple devices in a single substrate. The wide-scale production of small-scale structures can come true.

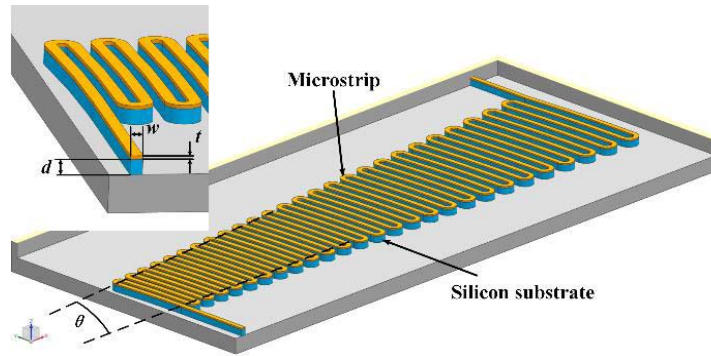


Figure 1. Conformal microstrip ALPML SWS model.

Compared with the dielectric-embedded MML SWS, this kind of structure which is a logarithmic-periodical structure has lower operation voltage, wider bandwidth and smaller dimension. Compared with conventional microstrip ALPML SWS, this novel kind of SWS can not only realize high coupling impedance, but also eliminate the charge accumulation.

This paper is organized as follows. In Section 2, the conformal microstrip ALPML SWS is described in detail, and high frequency characteristics are introduced. The transmission characteristics of conformal microstrip ALPML TWT are shown in Section 3. Section 4 presents the simulation results of beam-wave interaction of the conformal microstrip ALPML TWT. Finally, some useful conclusions are provided in the last section.

2. CONFORMAL MICROSTRIP LOG-PERIODIC MEANDER LINE SLOW WAVE STRUCTURE AND ITS HIGH FREQUENCY CHARACTERISTICS

2.1. Description of the Conformal Microstrip Log-Periodic Meander Line SWS and Fabrication Technology

According to the definition $r = ae^{b\varphi}$, the logarithmic spirals are determined by two important parameters a and b , in which a is the initial radius and b the spiral growth constant. The initial position is determined by initial radius a while the gap growth rate between two adjacent logarithmic spiral lines is determined by the spiral growth constant b . For angular log-periodic meander line, the angular θ shown in Fig. 2 also takes an important role in the dispersion of this structure.

$$\frac{v_r}{v_s} = \frac{e^{4b\pi} - 1}{(e^{2b\pi} + 1) \left[\frac{\sqrt{b^2 + 1}}{b} (e^{b\theta} - 1) + \frac{1}{2}\pi(e^{2b\pi} - e^{b\theta}) \right]} \quad (1)$$

where propagation velocity of wave along angular log-periodic meander line v_s is a constant for the microstrip meander line. According to Eq. (1), v_r is the radial component of v_s which is dependent on the values b and θ , and it is also the phase velocity in this structure. In Eq. ((1), parameter θ is given, and propagation velocity of wave v_s has been known. Therefore, the relationship between v_r and parameter b can be obtained from Eq. ((1). Value of v_r can be determined by operation parameter of TWT, so that the value of parameter b can be given. For the angular log-periodic SWS, the optimizing values of parameters are shown in Table 1. Some geometrical parameters are shown Fig. 3.

Table 1. Main dimensions of conformal microstrip ALPML SWS.

Parameter	Value
a	12 mm
b	0.0015
θ	5°
w (width)	0.06 mm
t (metal thickness)	0.01 mm
d (substrate thickness)	0.08 mm

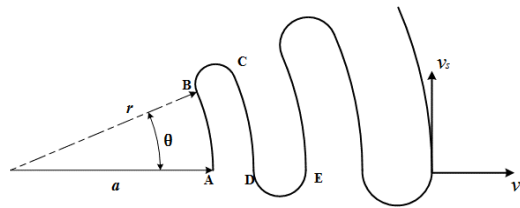


Figure 2. Angular log-periodic meander line.

The microfabrication technology DRIE is adopted to fabricate this structure. Firstly, the silicon is welded with a Mo metal support slice by silver paste. Secondly, plasma enhanced chemical vapor deposition is used to produce a copper film in the surface of silicon. Thirdly, the copper film and silicon substrate are etched under a photomask by a reactive ion etch. The fabricating structure is shown in Fig. 3(a). In the end, the remaining copper meander line is electroplated to increase the copper thickness. The finished prototype of conformal microstrip ALPML SWS is shown in Fig. 3(b).

2.2. Dispersion Characteristics

Due to the nonuniform periodicity of conformal microstrip ALPML SWS, the dispersion characteristics cannot be calculated by eigenmode algorithm. For calculating the dispersion characteristics of this

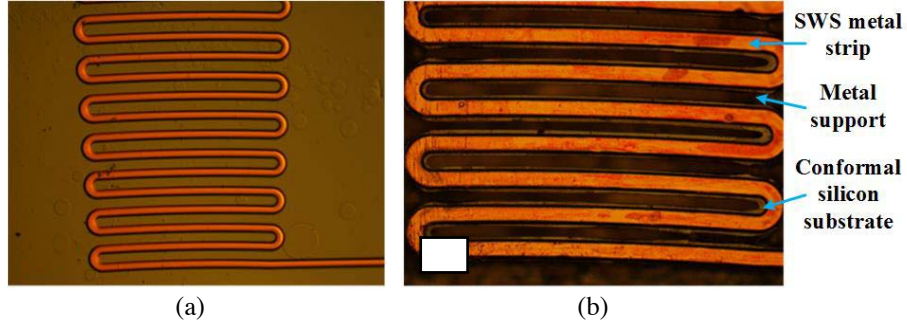


Figure 3. (a) The structure after DRIE and (b) conformal microstrip ALPML SWS after fabricating.

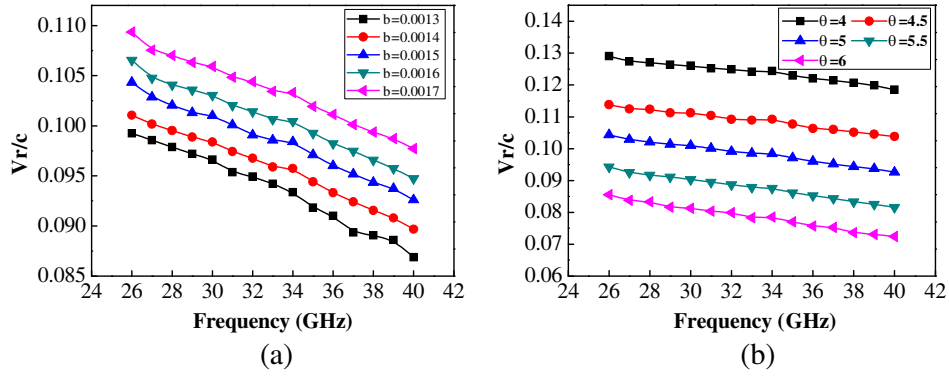


Figure 4. Dispersion curve with (a) different value b and (b) different value θ of conformal microstrip ALPML SWS.

structure, a novel algorithm has been proposed in [9].

The dispersion curves under different parameters b and θ , while the initial radius a is 12 mm, are shown in Fig. 4(a) and Fig. 4(b), respectively. Fig. 4(a) shows the positive correlation between v_r and parameter b , while Fig. 4(b) shows the negative correlation between v_r and parameter θ . For a constant conformal microstrip ALPML SWS, the dispersion curves are very flat, and it means that this structure has a broad bandwidth.

2.3. Coupling Impedance

As shown in Fig. 5(a), the vertical distance h is between the beam lower edge and the surface of the conformal microstrip SWS, which strongly affects the electric field intensity. It is clear from Fig. 5(b) and Fig. 5(c) that the electric field of both microstrip ALPML SWS and conformal microstrip ALPML is gradually decreasing while leaving the surface of the microstrip. Comparing the electric field distributions in the radial direction between conformal microstrip ALPML SWS and conventional one, we can see from Fig. 5(b) and Fig. 5(c) that the electric field distribution in the radial direction of conformal microstrip ALPML SWS is much higher than that of the conventional one.

On account of the nonuniform periodicity of conformal microstrip ALPML SWS, the coupling impedances of each period are different. The coupling impedances with different periodic numbers are shown in Fig. 6(a). With the increase of periodic number, the coupling impedance decreases. Meanwhile, as the distances h increases, the coupling impedances will decrease. As shown in Fig. 6(b), the average coupling impedances with different distances h is given. The coupling impedances in Fig. 6(b) are the average values with all different periodic numbers. As shown in Fig. 6(c), the coupling impedance of conformal ALPML SWS is over $9\ \Omega$ from 26 GHz to 40 GHz at $h = 0.08$ mm, and ~ 1.5 times as the conventional ALPML SWS.

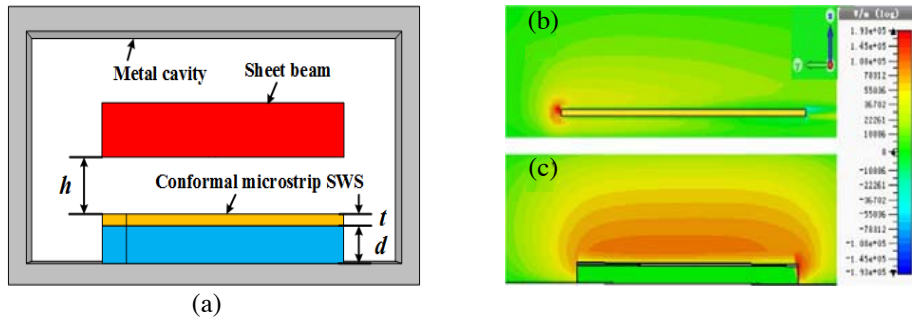


Figure 5. Cross-section of the model with sheet beam and E_z distribution of (b) conventional microstrip ALPML SWS and (c) conformal microstrip ALPML SWS.

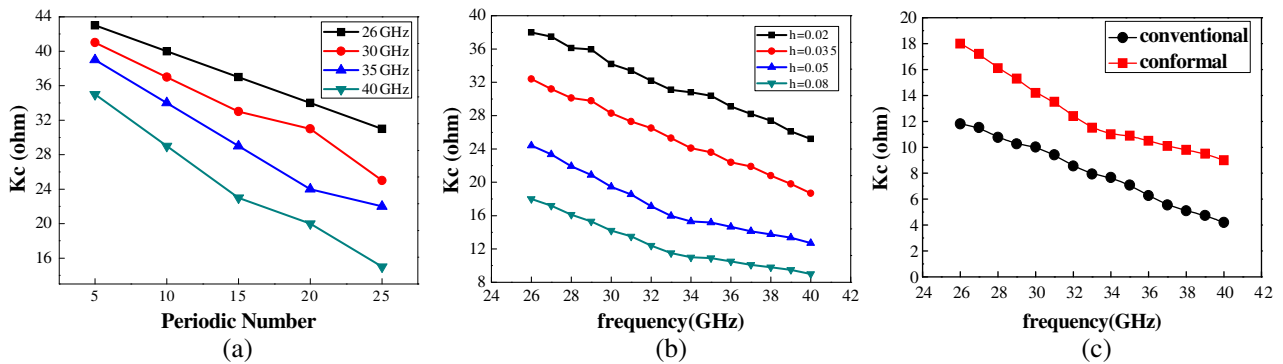


Figure 6. (a) Coupling impedances with different periodic number and (b) the average coupling impedances with different h , (c) average coupling impedances of conventional and conformal microstrip ALPML SWS at $h = 0.08$ mm.

3. TRANSMISSION CHARACTERISTICS OF THE WHOLE HIGH FREQUENCY SYSTEM

Figure 7 shows the model of conformal microstrip ALPML high frequency system with input/output coupler transition part. The ridge waveguides are adopted to be the input/output coupler. The ridge waveguides replace the coaxial line as the input/output coupler because of wide bandwidth and high power capacity.

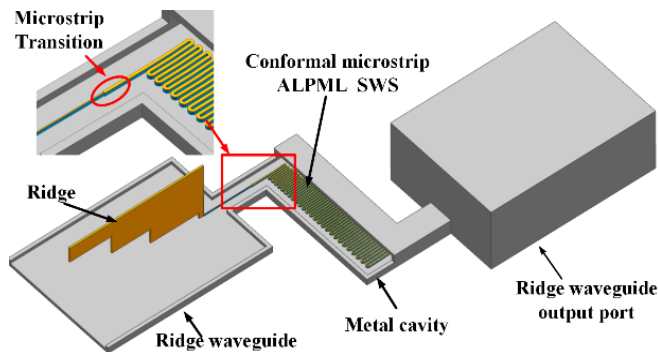


Figure 7. Conformal microstrip ALPML high frequency system with input/output coupler transition part.

In consideration of insertion loss between conformal microstrip and ridge waveguides, both of the impedances should be noted. The characteristic impedance of conformal microstrip ALPML SWS is 65.4Ω while the impedance of ridge waveguide is 118Ω [14]. In order to match the impedances, a conformal microstrip transition is designed to connect the ALPML SWS and ridge waveguide, as shown in Fig. 7. Decreasing the width of conformal microstrip to 0.02 mm can increase the value of the characteristic impedance.

The simulation transmission characteristics of conformal microstrip ALPML high frequency system with input/output coupler transition part are illustrated in Fig. 8. S_{11} of the whole structure is less than -14 dB from 27 to 39 GHz . And the transmission loss S_{21} is always greater than -1 dB in the Ka band.

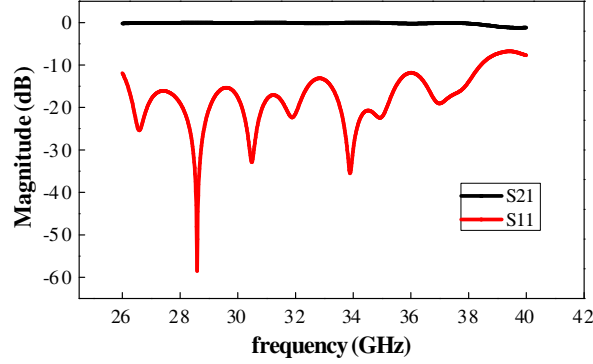


Figure 8. The transmission characteristic of conformal microstrip ALPML high frequency system with input/output coupler transition part.

4. BEAM-WAVE INTERACTION

The beam-wave interaction of the conformal microstrip ALPML TWT has been performed using CST Particle Studio [15]. The simulation parameters are given in Table 2. The cathode is designed as fan-shaped for obtaining the divergent radial sheet electron beam. The dimensions of the initial sheet beam are 0.2 mm in height and 1.1 mm in width. The beam voltage and beam current are 3600 V and 300 mA , respectively.

Table 2. Beam-wave interaction parameter.

Parameter	Value
Beam voltage	3600 V
Beam current	0.3 A
Beam emission area	$0.2\text{ mm} * 1.1\text{ mm}$
Frequency	35 GHz
Initial Input power	12 W
Radial magnetic field	0.2 T
Initial vertical distance h	0.02 mm

Two kinds of magnetic field can be used to focus the radial sheet beam. The first one is the radial magnetic field in [16], and the other is the PCM magnetic field in [11]. In this paper, the radial magnetic field is adopted to simplify the simulation. The Brillouin magnetic field calculation equation is given [17],

$$B_b^2 = \frac{I_0}{2\varepsilon_0\eta a_0(dr/dt)} = 5.4 \times 10^{-7} \frac{I}{\sqrt{V_a} a_0 r \theta} \quad (2)$$

where a_0 is the Brillouin half thickness, V_a the anode voltage, and I the beam current. According to Eq. (2), the Brillouin magnetic field $B_b = 0.08\text{ T}$.

As shown in Fig. 9(a), the radial magnetic field in which the magnetic flux density is 0.2 T is calculated by CST. The radial magnetic field component is nearly constant in Fig. 9(b). The axial and angular magnetic field components along the radial direction in Fig. 9(c) and Fig. 9(d) are so small that it is hard to affect the focusing of radial sheet beam.

As shown in Fig. 10, the electron beam moves forward, which is parallel to the surface of the conformal microstrip plane at $h = 0.02\text{ mm}$. The deflection of radial electron beam is weakened by using the radial divergent magnetic field. And the beam-wave interaction process is demonstrated clearly by the phenomenon that the electrons are retarded and accelerated periodically along the radial direction. Fig. 11 shows the electron phase space diagram. The electrons losing energy exceed those gaining energy, thus energy is transferred to the wave.

Figure 12 shows the saturated output power and saturated input power versus frequency. With the increase of frequency, the saturated input power decreases, and the saturated output power increases until reaching the maximum 220 W at 35 GHz , then the saturated output power decreases gradually.

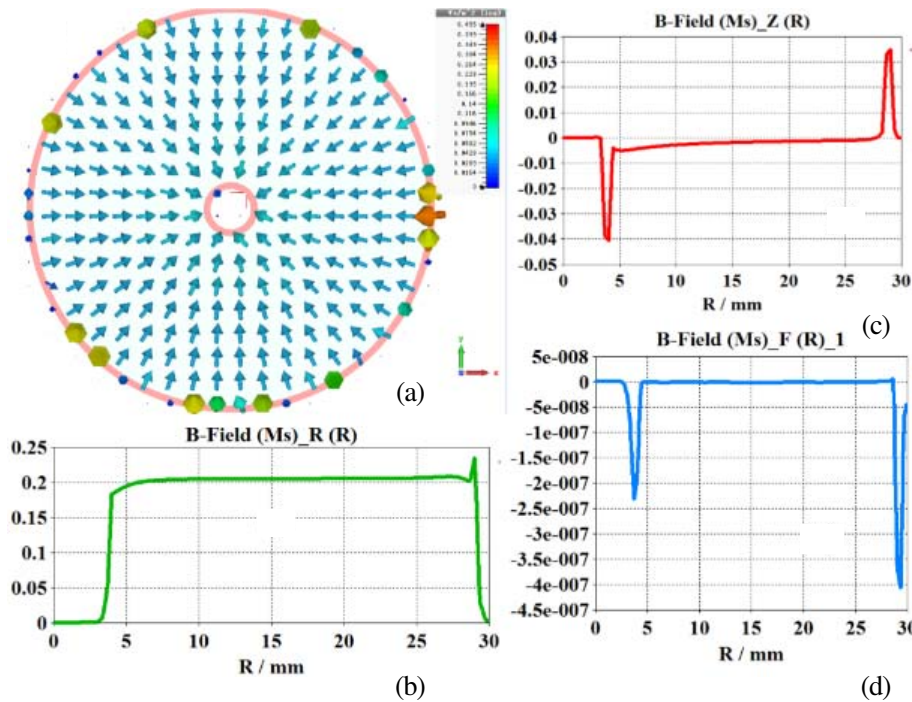


Figure 9. (a) Magnetic field B -field, (b) radial magnetic field component, (c) axial magnetic field and (d) angular magnetic field.

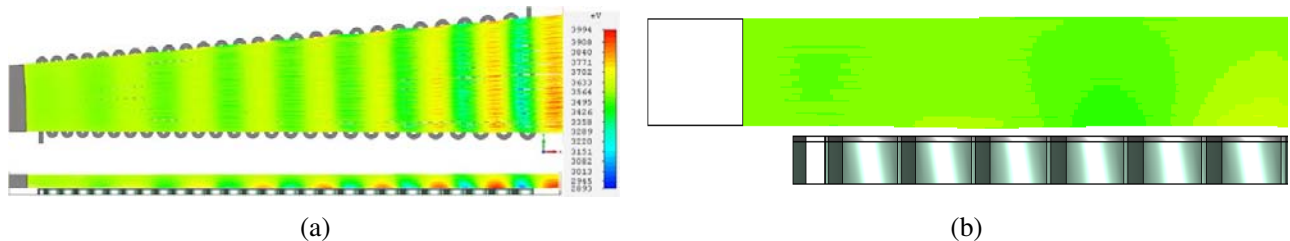


Figure 10. (a) The trajectory of radial beam and the electron beam bunching image and (b) the partial enlarged detail.

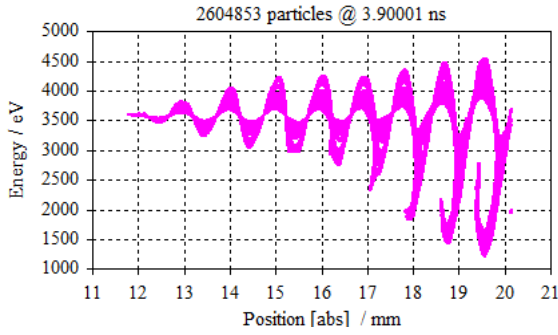


Figure 11. The electron phase space diagram.

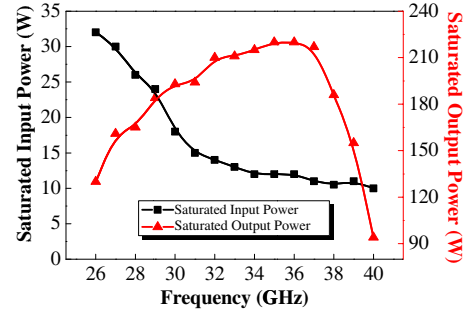


Figure 12. The saturated output power and saturated input power versus frequency.

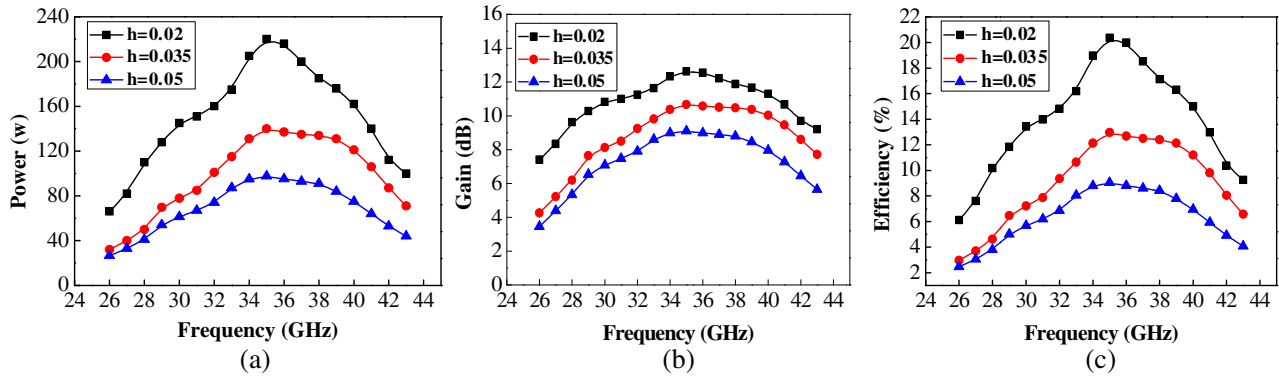


Figure 13. (a) The output power, (b) gain and (c) efficiency versus frequency with different vertical distances.

Figure 13 shows PIC simulation results of the conformal microstrip ALPML TWT with different parameter h when the other parameters are same. When the value of h is 0.02 mm, the best performance of the conformal microstrip ALPML TWT is obtained. The maximum output power and gain are about 220 W and 13 dB at 35 GHz. The maximum electron efficiency is 20% and greater than other microstrip TWTs. The 3-dB bandwidth ranges from 28 to 41 GHz. The output power is more than 120 W from 28 to 41 GHz. The electron efficiency of the conformal microstrip ALPML SWS reaches up to 12%. With the value of h increasing, the output power becomes smaller and smaller, and the gain and efficiency also decrease accordingly.

5. CONCLUSION

A conformal microstrip ALPML TWT is designed in this paper. The conformal microstrip plays an important role in the TWT to reduce the attenuation of dielectric substrate, enhance the coupling impedance and beam-wave interaction efficiency and eliminate the charge accumulation. The output power can approach 220 W with the gain of 13 dB when the beam voltage, beam current and input power are 3600 V, 0.3 A, and 12 W, respectively. The maximum electron efficiency can reach 20%. The 3 dB bandwidth is 14 GHz ranging from 28 GHz to 41 GHz.

ACKNOWLEDGMENT

This work was supported by the National Natural Science Foundation of China (Grant No. 61531010).

REFERENCES

1. Rappaport, T. S., S. Sun, R. Mayzus, H. Zhao, Y. Azar, K. Wang, G. N. Wong, J. K. Schulz, M. Samimi, and F. Gutierrez, "Millimeter wave mobile communications for 5G cellular: It will work!," *IEEE Access*, Vol. 1, 335–349, May 2013, DOI:10.1109/ACCESS.2013.2260813.
2. Nurmela, V., A. Karttunen, and A. Roivainen, "Mobile and wireless communications enablers for the twenty-twenty information society," Deliverable D1. 4, V1. 0, ICT-317669, METIS project, 2015.
3. Tehrani, M., M. Uysal, and H. Yanikomeroglu, "Device-to-device communication in 5G cellular networks: Challenges, solutions, and future directions," *IEEE Commun. Mag.*, Vol. 52, No. 5, 86–92, May 2014, DOI: 10.1109/MCOM.2014.6815897.
4. Andrews, J. G., S. Buzzi, W. Choi, S. V. Hanly, A. Lozano, A. C. K. Soong, and J. C. Zhang, "What will 5G be?," *IEEE J. Sel. Areas Commun.*, Vol. 32, No. 6, 1065–1082, Jun. 2014, DOI: 10.1109/JSAC.2014. 2328098.
5. Shen, F., Y. Wei, H. Yin, Y. Gong, X. Xu, S. Wang, W. Wang, and J. Feng, "A novel V-shaped microstrip meander-line slow-wave structure for W-band MMPM," *IEEE Trans. Plasma Sci.*, Vol. 40, No. 2, 463–469, Feb. 2012, DOI: 10.1109/TPS.2011.2175252.
6. Larsen, P. B., D. K. Abe, S. J. Cooke, B. Levush, T. M. Antonsen, Jr., and R. E. Myers, "Characterization of a Ka-band Sheet-Beam structure coupled-cavity slow-wave," *IEEE Trans. Plasma Sci.*, Vol. 38, No. 6, 1244–1254, Jun. 2010, DOI: 10.1109/TPS.2010.2043690.
7. Datta, S. K., V. B. Naidu, S. U. Reddy, L. Kumar, and B. N. Basu, "Analytical exploration of ultrawideband helix slow-wave structures using multidispersion phase velocity taper," *IEEE Trans. Plasma Sci.*, Vol. 37, No. 2, 311–316, Feb. 2009, DOI: 10.1109/TPS.2008.2010548.
8. Savel'yev, V. S. and G. I. Kushcenko, "Experimental investigation of a TWT with a radial electron stream," *Radio Eng. Electron. Phys.*, Vol. 15, No. 12, 2267–2272, 1970.
9. Wang, S., Y. Gong, Y. Hou, Z. Wang, Y. Wei, Z. Duan, and J. Cai, "Study of a log-periodic slow wave structure for ka-band radial sheet beam traveling wave tube," *IEEE Trans. Plasma Sci.*, Vol. 41, No. 8, 2277–2282, Aug. 2013, DOI: 10.1109/TPS.2013.2271639.
10. Li, X., Y. Xu, S. Wang, Z. Wang, X. Shi, Z. Duan, Y. Wei, J. Feng, and Y. Gong, "Study on phase velocity tapered microstrip angular log-periodic meander line travelling wave tube," *IET Microwaves, Antennas Propag.*, Vol. 10, No. 8, 902–907, 2016, DOI: 10.1049/iet-map.2015.0520.
11. Li, X., Z. Wang, T. He, H. Gong, Z. Duan, Y. Wei, and Y. Gong, "Study on radial sheet beam electron optical system for miniature low-voltage traveling-wave tube," *IEEE Trans. Electron Devices*, Vol. 64, No. 8, 3405–3412, Aug. 2017, DOI: 10.1109/TED.2017.2711616.
12. Ding, C., Y. Wei, Q. Li, L. Zhang, G. Guo, and Y. Gong, "A dielectric-embedded microstrip meander line slow-wave structure for miniaturized traveling wave tube," *Journal of Electromagnetic Waves and Applications*, Vol. 31, No. 17, 1938–1946, Nov. 2017, DOI: 10.1080/09205071.2017.1358109.
13. Sengele, S., H. Jiang, J. H. Booske, C. L. Kory, D. W. van der Weide, and R. L. Ives, "Microfabrication and characterization of a selectively metallized w-band meander-line TWT circuit," *IEEE Trans. Electron Devices*, Vol. 56, No. 5, 730–737, May 2009, DOI: 10.1109/TED.2009.2015416.
14. Sun, W. and C. A. Balanis, "MFIE analysis and design of ridged waveguides," *IEEE Trans. Microw. Theory Tech.*, Vol. 41, No. 11, 1965–1971, Nov. 1993, DOI: 10.1109/22.273423.
15. CST, "CST STUDIO SUITE help documentation," 2014.
16. Wang, S., Y. Gong, Z. Wang, Y. Wei, Z. Duan, and J. Feng, "Study of the symmetrical microstrip angular log-periodic meander-line traveling-wave tube," *IEEE Trans. Plasma Sci.*, Vol. 44, No. 9, 1787–1793, Sept. 2016, Doi: 10.1109/TPS.2016.2598614.
17. Wang, S., Y. Gong, Y. Wei, and Z. Duan, "Study on the radial-sheet-beam electron optical system," *IEEE Trans. Plasma Sci.*, Vol. 40, No. 12, 3442–3448, Dec. 2012, DOI: 10.1109/TPS.2012.2218623.